Propulsion System Integration and Design

Computational Techniques I
Internal Flow

The University of Kansas
May 23–27, 1994

Charles E. Towne

NASA Lewis Research Center
Internal Fluid Mechanics Division
Cleveland, Ohio

PROPULSION SYSTEM INTEGRATION AND DESIGN

Computational Techniques I
Internal Flow

Charles E. Towne

NASA Lewis Research Center
Internal Fluid Mechanics Division
Cleveland, Ohio

1. INTRODUCTION

Interest in the use of computational fluid dynamics (CFD) for the design and analysis of propulsion system components has increased greatly in the past few years. Several factors have contributed to this growth, including: (1) complex geometric design requirements for many modern propulsion systems, leading to flow phenomena that may not be intuitively predictable; (2) increasing fuel costs, leading to potentially large cost savings for even small performance improvements; (3) the high cost and/or lack of facilities for extensive experimental testing; (4) the continued development and improvement of sophisticated numerical algorithms for solving the complex equations governing fluid flow; and (5) the increasing availability of supercomputers.

Many different computational methods have been and continue to be used for studying internal flow. To effectively utilize these computational tools, today's designer must be aware of the types of methods that are applicable to a specific problem, and of their capabilities and limitations.

The object of this presentation, therefore, is to remove some of the mystery from CFD by systematically discussing the various types of analyses commonly used for internal flows. (It should be noted that much of the material in this presentation also applies to external flows.) The fundamental equations governing fluid flow will be presented first, followed by a brief introduction to solution methods used in CFD. Then, each analysis method, from potential flow to time-averaged Navier-Stokes, will be discussed. For each analysis, the emphasis will be on the simplifying assumptions made in deriving the governing equations, the resulting features and limitations of the analysis, and the types of geometries and flow situations it can successfully compute. Examples of computed results will be shown. The talk will conclude with a summary of the current overall status of CFD in propulsion research, and the problem areas limiting their use in a design environment.

2. FUNDAMENTAL EQUATIONS

The fundamental governing equations for fluid flow are presented below. The basic conservation laws, in differential form, for mass, momentum, and energy, may be written as follows:

$$\frac{\partial \rho}{\partial t} + \frac{\partial (\rho u)}{\partial x} + \frac{\partial (\rho v)}{\partial y} = 0 \tag{2-1}$$

$$\frac{\partial (\rho u)}{\partial t} + \frac{\partial (\rho u^2)}{\partial x} + \frac{\partial (\rho uv)}{\partial y} = -\frac{\partial p}{\partial x} + \frac{1}{Re_r}\left(\frac{\partial \tau_{xx}}{\partial x} + \frac{\partial \tau_{xy}}{\partial y}\right) \tag{2-2}$$

$$\frac{\partial (\rho v)}{\partial t} + \frac{\partial (\rho uv)}{\partial x} + \frac{\partial (\rho v^2)}{\partial y} = -\frac{\partial p}{\partial y} + \frac{1}{Re_r}\left(\frac{\partial \tau_{xy}}{\partial x} + \frac{\partial \tau_{yy}}{\partial y}\right) \tag{2-3}$$

$$\frac{\partial(E_T)}{\partial t} + \frac{\partial(uE_T)}{\partial x} + \frac{\partial(vE_T)}{\partial y} = -\frac{\partial(up)}{\partial x} - \frac{\partial(vp)}{\partial y} - \frac{1}{Re_r Pr_r}\left(\frac{\partial q_x}{\partial x} + \frac{\partial q_y}{\partial y}\right) + \frac{1}{Re_r}\left[\frac{\partial}{\partial x}(u\tau_{xx} + v\tau_{xy}) + \frac{\partial}{\partial y}(u\tau_{xy} + v\tau_{yy})\right] \tag{2-4}$$

In order, these equations are commonly called the continuity, *x*-momentum, *y*-momentum, and energy equations. For simplicity, they have been written in a 2-D Cartesian coordinate system. Several different versions of the energy equation appear in the literature. One often seen uses total enthalpy as the dependent variable, and may be written as

$$\frac{\partial(\rho H)}{\partial t} + \frac{\partial(\rho uH)}{\partial x} + \frac{\partial(\rho vH)}{\partial y} = -\frac{1}{Re_r Pr_r}\left(\frac{\partial q_x}{\partial x} + \frac{\partial q_y}{\partial y}\right) + \frac{1}{Re_r}\left[\frac{\partial}{\partial x}(u\tau_{xx} + v\tau_{xy}) + \frac{\partial}{\partial y}(u\tau_{xy} + v\tau_{yy})\right] \tag{2-5}$$

The shear stresses and heat fluxes are given by

$$\tau_{xx} = 2\mu\frac{\partial u}{\partial x} + \lambda\left(\frac{\partial u}{\partial x} + \frac{\partial v}{\partial y}\right) \tag{2-6}$$

$$\tau_{yy} = 2\mu\frac{\partial v}{\partial y} + \lambda\left(\frac{\partial u}{\partial x} + \frac{\partial v}{\partial y}\right) \tag{2-7}$$

$$\tau_{xy} = \mu\left(\frac{\partial u}{\partial y} + \frac{\partial v}{\partial x}\right) \tag{2-8}$$

$$q_x = -k\frac{\partial T}{\partial x} \tag{2-9}$$

$$q_y = -k\frac{\partial T}{\partial y} \tag{2-10}$$

An equation of state is also needed to relate pressure, temperature, and density. Typically, a perfect gas is assumed, and the equation is simply

$$p = \rho RT \tag{2-11}$$

For calorically perfect gases, this can be rewritten as

$$p = (\gamma - 1)\left[E_T - \frac{1}{2}\rho(u^2 + v^2)\right] \tag{2-12}$$

In the above equations, the independent variables are the time t, and the Cartesian coordinates x and y. The four primary dependent variables are the density ρ, the velocities u and v in the x and y directions, and either the total energy per unit volume E_T or the total enthalpy H. The total energy and total enthalpy may be defined in terms of more familiar parameters as follows:

$$E_T = \rho c_v T + \frac{1}{2}\rho(u^2 + v^2) \tag{2-13}$$

$$H = c_p T + \frac{1}{2}(u^2 + v^2) \tag{2-14}$$

Additional variables appearing in these equations are the pressure p, the temperature T, the coefficient of viscosity μ, the second coefficient of viscosity λ (usually defined as $\lambda = -2\mu/3$), the coefficient of thermal conductivity k, the specific heat coefficients c_p and c_v, the ratio of specific heats $\gamma = c_p/c_v$, and the gas constant R. Additional equations may be needed to define μ, k, and c_p in terms of temperature for the gas under consideration.

All of the equations have been nondimensionalized using appropriate normalizing conditions. Lengths have been nondimensionalized by L_r, velocities by u_r, density by ρ_r, temperature by T_r, viscosity by μ_r, thermal conductivity by k_r, pressure and total energy by $\rho_r u_r^2$, time by L_r/u_r, and gas constant and specific heat by u_r^2/T_r. The reference Reynolds and Prandtl numbers are thus defined as $Re_r = \rho_r u_r L_r/\mu_r$ and $Pr_r = \mu_r u_r^2/k_r T_r$. Note that this Prandtl number does not have a physically meaningful value, but is merely defined by a combination of the normalizing conditions for c_p, μ, and k that appear when the equations are nondimensionalized.

These fundamental equations have been written in what is called conservation, or divergence, form. This means that the coefficients are either constant or, if variable, that their derivatives do not appear. In vector form, the divergence of a physical quantity can be easily identified in these equations. For example, equation (2-1), the continuity equation, may be written as

$$\frac{\partial \rho}{\partial t} + \nabla \cdot \rho \vec{V} = 0 \tag{2-15}$$

The nonconservative form of the continuity equation would be

$$\frac{\partial \rho}{\partial t} + \rho \frac{\partial u}{\partial x} + u \frac{\partial \rho}{\partial x} + \rho \frac{\partial v}{\partial y} + v \frac{\partial \rho}{\partial y} = 0 \tag{2-16}$$

Writing the equations in conservation form helps avoid some numerical problems that can occur when solving problems with discontinuities, such as shock waves. It also simplifies the task of developing a numerical solution procedure that conserves mass, momentum, and energy. This second point is discussed further in the next section.

Although, strictly speaking, the term ‘‘Navier-Stokes’’ applies only to the two momentum equations, all four equations as a set are generally referred to as the Navier-Stokes equations. They completely describe the motion of any continuum flow of a Newtonian fluid. Body forces and internal heat addition have been assumed negligible. However, these terms could also be included.

Turbulence can also be computed with these equations. With current and foreseeable computers, however, it’s not feasible to resolve the small time and length scales required to actually compute turbulence for realistic propulsion system problems. Turbulence is therefore modeled using various assumptions. With the turbulence models used for practical engineering problems, the viscosity and thermal conductivity coefficients μ and k are locally increased to account for the increased diffusion due to turbulence. They are then known as ‘‘effective’’ viscosity and thermal conductivity coefficients. The result is that the Navier-Stokes equations normally used for turbulent flow look exactly like the ones shown here.

These equations are a coupled set of nonlinear second-order partial differential equations, and are therefore very difficult to solve. Closed form solutions exist only for a few very simplified cases. To solve more realistic fluid flow problems, assumptions are usually made about the flow that allow these equations to be simplified.

3. NUMERICAL METHODS

Before presenting the various types of analyses that may be derived from the fundamental equations, a short discussion on the types of numerical methods used in CFD may be useful. It should be noted that the material in this section is only a basic introduction. There are many different solution procedures being used today. For more detailed information see the books by Anderson, Tannehill, and Pletcher (1984), Baker (1983), Fletcher (1988), and Hoffmann (1989).

3.1 Finite Difference Methods

The most common solution procedures being used today in CFD are finite difference methods. In a finite difference method, the derivatives in the governing equations are approximated by finite difference formulas. The resulting finite difference equations are algebraic, and can be solved on a digital computer.

3.1.1 Computational Mesh

The first step in using a finite difference method is to construct a finite difference mesh in the flow domain of interest, as shown in the following figure for a simple two-dimensional square domain.

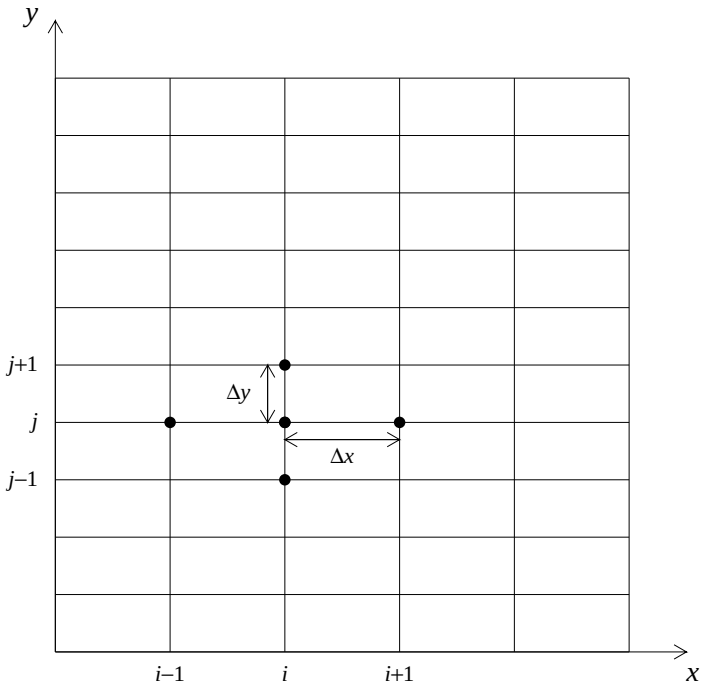

Computational mesh.

In this mesh, the Cartesian coordinates x and y both vary from 0 to 1, and the mesh is evenly spaced in both directions, although Δx need not be equal to Δy. The grid points are labeled with the indices i and j in the x and y directions, respectively.

Of course, in real-world applications the flow domain is not normally square. And it's usually desirable to cluster grid points in certain regions of the flow. For example, in a viscous analysis grid points should be concentrated near solid boundaries for proper resolution of the steep gradients in the boundary layers. Therefore, the governing differential equations are typically transformed from an unevenly spaced x, y coordinate system in physical space to an evenly spaced ξ, η coordinate system in computational space. The transformed equations are then actually solved on an evenly spaced square grid in computational space. In this discussion, we can thus use the simple mesh shown in the figure, with no loss in generality.

3.1.2 Finite Difference Formulas

The finite difference formulas used to approximate the derivatives in the governing differential equations may be derived using Taylor series expansions. For example, given a function $f(x, y)$, the value of f at the point $(x + \Delta x, y)$ may be found by expanding f in a Taylor series about the point (x, y) as follows:

$$f(x+\Delta x, y) = f(x, y) + \Delta x \frac{\partial f}{\partial x} + \frac{(\Delta x)^2}{2!} \frac{\partial^2 f}{\partial x^2} + \frac{(\Delta x)^3}{3!} \frac{\partial^3 f}{\partial x^3} + \cdots \tag{3-1}$$

Solving for $\partial f / \partial x$,

$$\frac{\partial f}{\partial x} = \frac{f(x+\Delta x, y) - f(x,y)}{\Delta x} - \frac{\Delta x}{2!}\frac{\partial^2 f}{\partial x^2} - \frac{(\Delta x)^2}{3!}\frac{\partial^3 f}{\partial x^3} + \cdots$$

or,

$$\frac{\partial f}{\partial x} = \frac{f(x+\Delta x, y) - f(x,y)}{\Delta x} + O(\Delta x)$$

where the notation $O(\Delta x)$ is used to represent the sum of all the terms of order Δx and higher. This can be written somewhat more compactly using subscripts to represent locations in the finite difference mesh, as follows:

$$\left(\frac{\partial f}{\partial x}\right)_{i,j} = \frac{f_{i+1,j} - f_{i,j}}{\Delta x} + O(\Delta x) \tag{3-2}$$

This is the first-order forward difference formula for approximating $\partial f/\partial x$. The term $O(\Delta x)$ is the truncation error.

A first-order backward difference formula may be derived by using a Taylor series expansion for at the point $(x - \Delta x, y)$.

$$f(x-\Delta x, y) = f(x,y) - \Delta x\frac{\partial f}{\partial x} + \frac{(\Delta x)^2}{2!}\frac{\partial^2 f}{\partial x^2} - \frac{(\Delta x)^3}{3!}\frac{\partial^3 f}{\partial x^3} + \cdots \tag{3-3}$$

Solving for $\partial f/\partial x$, and using index notation,

$$\left(\frac{\partial f}{\partial x}\right)_{i,j} = \frac{f_{i,j} - f_{i-1,j}}{\Delta x} + O(\Delta x) \tag{3-4}$$

By subtracting equation (3-3) from (3-1), we get

$$f(x+\Delta x, y) - f(x-\Delta x, y) = 2\Delta x\frac{\partial f}{\partial x} + 2\frac{(\Delta x)^3}{3!}\frac{\partial^3 f}{\partial x^3} + \cdots \tag{3-5}$$

Solving for $\partial f/\partial x$, and using index notation,

$$\left(\frac{\partial f}{\partial x}\right)_{i,j} = \frac{f_{i+1,j} - f_{i-1,j}}{2\Delta x} + O(\Delta x)^2 \tag{3-6}$$

This is the second-order centered difference formula for $\partial f/\partial x$.

Adding equations (3-1) and (3-3) gives

$$f(x+\Delta x, y) + f(x-\Delta x, y) = 2f(x,y) + 2\frac{(\Delta x)^2}{2!}\frac{\partial^2 f}{\partial x^2} + \cdots \tag{3-7}$$

This can be solved for $\partial^2 f/\partial x^2$. Using index notation,

$$\left(\frac{\partial^2 f}{\partial x^2}\right)_{i,j} = \frac{f_{i+1,j} - 2f_{i,j} + f_{i-1,j}}{(\Delta x)^2} + O(\Delta x)^2 \tag{3-8}$$

This is a second-order centered difference formula for $\partial^2 f/\partial x^2$.

A second-order centered difference formula for mixed partial derivatives may be derived by first noting that

$$\frac{\partial^2 f}{\partial x \partial y} = \frac{\partial}{\partial x}\left(\frac{\partial f}{\partial y}\right)$$

Using equation (3-6) for $\partial f/\partial y$,

$$\left(\frac{\partial^2 f}{\partial x \partial y}\right)_{i,j} = \frac{\partial}{\partial x}\left(\frac{f_{i,j+1} - f_{i,j-1}}{2\Delta y}\right) + O(\Delta y)^2$$

Using equation (3-6) again, for the $\partial/\partial x$ terms, we get

$$\left(\frac{\partial^2 f}{\partial x \partial y}\right)_{i,j} = \frac{f_{i+1,j+1} - f_{i-1,j+1} - f_{i+1,j-1} + f_{i-1,j-1}}{4\Delta x \Delta y} + O[(\Delta x)^2, (\Delta y)^2] \tag{3-9}$$

3.1.3 Explicit Solution Procedures

To actually solve a partial differential equation, the finite difference formulas derived in the previous section are used to approximate each derivative in the differential equation. As a simple example, consider the one-dimensional unsteady heat conduction equation.

$$\frac{\partial T}{\partial t} = \alpha \frac{\partial^2 T}{\partial x^2} \tag{3-10}$$

Here T is the temperature and $\alpha = k/\rho c_p$ is the thermal diffusivity.

To solve this equation, we could evaluate equation (3-10) at time level n, where the temperature is assumed known. Using first-order forward differencing for the time derivative, and second-order central differencing for the diffusion term, equation (3-10) may be approximated by the following finite difference equation:

$$\frac{T_i^{n+1} - T_i^n}{\Delta t} = \alpha \frac{T_{i+1}^n - 2T_i^n + T_{i-1}^n}{(\Delta x)^2} \tag{3-11}$$

Note that the time level is denoted by a superscript, and the spatial location is denoted by a subscript. This seems to be a standard convention for finite difference methods.

The only unknown in this equation is T_i^{n+1}. This is called an *explicit* method. The solution can be advanced in time by writing equation (3-11) at each grid point i, and solving each of the resulting equations for T_i^{n+1} independently.

Explicit methods have successfully been used in a wide variety of CFD applications. The biggest advantage of explicit methods is simplicity. They are relatively easy to understand and to program. They do have one big disadvantage, however. It can be shown that, for a stable solution, the time step Δt must be less than some limiting value that depends on the spatial grid spacing. The smaller the grid spacing, the smaller Δt must be. This is the well-known Courant-Friedrichs-Lewy (CFL) condition.

3.1.4 Implicit Solution Procedures

Instead of evaluating equation (3-10) at time level n, suppose we evaluate it at time level $n+1$, where the temperature is unknown. Using first-order backward differencing for the time derivative, and second-order central differencing for the diffusion term, we get

$$\frac{T_i^{n+1} - T_i^n}{\Delta t} = \alpha \frac{T_{i+1}^{n+1} - 2T_i^{n+1} + T_{i-1}^{n+1}}{(\Delta x)^2} \tag{3-12}$$

There are three unknowns in this equation — T_{i-1}^{n+1}, T_i^{n+1}, and T_{i+1}^{n+1}. This is called an *implicit* method. We can rearrange equation (3-12) in the following form:

$$a_i T_{i-1}^{n+1} + b_i T_i^{n+1} + c_i T_{i+1}^{n+1} = S_i^n \tag{3-13}$$

where the coefficients of the unknowns have been collected into a_i, b_i, and c_i, and known terms have been collected into the source term S_i^n. When equation (3-13) is written at each grid point i, the result is a set of coupled algebraic equations that must be solved simultaneously. In matrix form, these equations have a tridiagonal coefficient matrix, which is very common in finite difference CFD methods. Fortunately, there are very efficient solution procedures for tridiagonal systems of equations.

Like explicit methods, implicit methods have also successfully been used in a wide variety of CFD applications. Implicit methods are more difficult to program and require more computer time per time step than explicit methods, but do not have a stability limit on the size of the time step. (At least in theory, for simple equations. There is no exact stability theory for more complicated equations, like the compressible Navier-Stokes equations. In practice, it's often found through experience that there is a limit on the time step size, even for implicit methods. It's typically larger than the limit for explicit methods, however.) The trend today seems to be toward implicit methods.

3.1.5 Extension to Systems of Equations and Multiple Dimensions

The above discussion is for a single governing equation in one dimension. The extension to systems of equations is straightforward for explicit methods. For implicit methods, the situation is more complicated. For systems of coupled governing equations, which are common in CFD, the equivalent to equation (3-13) is a matrix equation. For a system of four equations, the coefficients a, b, and c are 4×4 matrices, and the unknown dependent variable T and the source term S are 4-element vectors. When written for all the grid points, the result is a block tridiagonal system, instead of a scalar tridiagonal system.

The extension to two- or three-dimensional problems is again fairly straightforward for explicit methods. For implicit methods, each time step is usually split into sub-steps, one in each of the coordinate directions. These solution algorithms are called alternating-direction-implicit (ADI) methods.

3.1.6 Conservative Property of a Solution Procedure

In CFD, the governing differential equations express the basic conservation laws at a point in space. If these equations could be solved by integrating over all points in space (''all'' being infinite), mass, momentum, and energy would be automatically conserved. Unfortunately, when the equations are solved numerically, we can't use an infinite number of points. We therefore have to worry about whether or not mass, momentum, and energy are conserved in the numerical solution.

Suppose we applied the integral form of the conservation laws to the entire flow field. By integrating numerically using the grid points on the boundaries of the flow domain, we could develop a discretized form of the integral conservation laws. Suppose we then write the finite difference representation of the governing differential equations at every grid point in the flow domain, and sum them all up. If the terms at the interior grid points all cancel, and the remaining terms are exactly the same as those in the discretized form of the integral conservation laws, the numerical procedure is said to be conservative.

Note the distinction between the conservative property of the numerical procedure, and the conservation form for the governing differential equations, discussed in the previous section. Writing the differential equations in conservation form is important for flows with discontinuities, like shock waves. It does not, by itself, imply that the numerical solution will automatically conserve mass, momentum, and energy. It does, however, make it relatively easy to construct numerical procedures that do have the conservative property.

3.2 Other Methods

Besides finite difference methods, many other methods have been used in CFD. Some of these, like panel methods, the method of characteristics, or integral methods, are specialized methods used in a particular type of CFD analysis, and will be mentioned in subsequent sections. There are a couple of other general solution methods that will be mentioned very briefly here, however. These are newer and not as widely used in CFD as finite difference methods, but they do have some strong advocates.

3.2.1 Finite Volume Methods

In finite difference methods, the starting point is a set of partial differential equations that represent the basic conservation laws in *differential* form. The algebraic equations that are ultimately solved are derived by using finite difference formulas to approximate the derivatives in the differential equations.

Finite volume methods, on the other hand, start with the basic conservation laws in *integral* form. These laws are applied to a control volume surrounding a grid point in the computational mesh. By doing this for every grid point, and summing, a set of algebraic equations is derived that can be solved for the unknown flow variables.

It can be seen that finite volume methods take the discrete nature of the numerical problem into account from the very beginning. They are conservative by their very nature. They also allow complicated flow domains to be discretized relatively easily, without the need for a transformation between physical and computational space.

3.2.2 Finite Element Methods

Finite element methods are part of a more general class called weighted residual methods. (Finite volume methods can also be classified as weighted residual methods, but they actually resemble finite difference methods when implemented.) A weighted residual method assumes that the solution may be represented analytically.

To illustrate, we again use the one-dimensional heat conduction equation, equation (3-10), as an example. Following the discussion in Volume 1 of Fletcher (1988), in a weighted residual method an approximate, or trial, solution of equation (3-10) would be represented as

$$T = \sum_{j=1}^{J} a_j(t)\phi_j(x) \tag{3-14}$$

where $a_j(t)$ are unknown coefficients, and $\phi_j(x)$ are known analytic functions called trial functions. The larger J is, the more accurate the solution will be.

Substituting equation (3-14) into (3-10) and rearranging yields

$$\frac{\partial T}{\partial t} - \alpha \frac{\partial^2 T}{\partial x^2} = \frac{\partial}{\partial t}\left(\sum_{j=1}^{J} a_j(t)\phi_j(x)\right) - \alpha \frac{\partial^2}{\partial x^2}\left(\sum_{j=1}^{J} a_j(t)\phi_j(x)\right) = R \tag{3-15}$$

Since T is an approximate solution, it does not exactly satisfy equation (3-10). R is called the residual.

The unknowns $a_j(t)$ are found by requiring that

$$\int W_m(x) R dx = 0 \tag{3-16}$$

where the integral is over the computational domain, and $m = 1, 2, \cdots, M$. This represents a system of M equations for the J unknowns a_j. For a well-posed problem, of course, we must choose $M = J$. The choice of the weighting functions W_m determines which method in the class of weighted residual methods is being used. If the weighting functions are the same as the trial functions, i.e., if $W_m(x) = \phi_m(x)$, this is called a Galerkin method. Most finite element CFD methods are Galerkin methods.

Up to now, this discussion has been about weighted residual methods in general. Finite element methods have two particular additional features. First, the unknown coefficients $a_j(t)$ are taken as the unknown values of the dependent variable T at a set of nodes in the flow domain. Thus, equation (3-14) becomes

$$T = \sum_{j=1}^{J} T_j(t)\phi_j(x) \tag{3-17}$$

The second feature of a finite element method is that the trial functions $\phi_j(x)$ are simply interpolating functions to represent values between node points. These interpolating functions are usually linear, but quadratic functions are

also used.

To summarize, in a finite element method the unknown dependent variables are represented by a continuous analytical function. This function is constructed using the unknowns at discrete nodes in the flow domain, with interpolating functions to represent the values of the dependent variables between node points. You end up with a system of J algebraic equations to solve for the J unknown dependent variables, where J is the number of nodes in the flow domain. Finite element methods have traditionally been particularly good for complicated flow domains, since the nodes need not be based on a uniform rectangular grid.

4. POTENTIAL FLOW ANALYSES

4.1 Assumptions Made

Potential flow analyses are among the oldest and most well established methods currently being used for internal flow. The flow must be irrotational (i.e., the vorticity $\nabla \times \vec{V}$ is assumed to be zero). Except for a few very specialized flow situations, viscosity introduces vorticity into the flow. The flow is therefore assumed to be inviscid. The flow is also assumed to be steady and isentropic.

The following equations relate the assumptions made for potential flow to the terms in the Navier-Stokes equations, showing the terms that are eliminated. (Note that, since the flow is steady, the time derivatives have also been eliminated.)

$$\frac{\partial(\rho u)}{\partial x} + \frac{\partial(\rho v)}{\partial y} = 0 \tag{4-1}$$

$$\frac{\partial(\rho u^2)}{\partial x} + \frac{\partial(\rho uv)}{\partial y} = -\frac{\partial p}{\partial x} + \cancel{\frac{1}{Re_r}\left(\frac{\partial \tau_{xx}}{\partial x} + \frac{\partial \tau_{xy}}{\partial y}\right)} \tag{4-2}$$

$$\frac{\partial(\rho uv)}{\partial x} + \frac{\partial(\rho v^2)}{\partial y} = -\frac{\partial p}{\partial y} + \cancel{\frac{1}{Re_r}\left(\frac{\partial \tau_{xy}}{\partial x} + \frac{\partial \tau_{yy}}{\partial y}\right)} \tag{4-3}$$

$$\frac{\partial(uE_T)}{\partial x} + \frac{\partial(vE_T)}{\partial y} = -\frac{\partial(up)}{\partial x} - \frac{\partial(vp)}{\partial y} - \cancel{\frac{1}{Re_r Pr_r}\left(\frac{\partial q_x}{\partial x} + \frac{\partial q_y}{\partial y}\right)}$$

$$+\cancel{\frac{1}{Re_r}\left[\frac{\partial}{\partial x}(u\tau_{xx} + v\tau_{xy}) + \frac{\partial}{\partial y}(u\tau_{xy} + v\tau_{yy})\right]} \tag{4-4}$$

$$\nabla \times \vec{V} = 0 \quad \rightarrow \quad \nabla \phi = \vec{V} \tag{4-5}$$

Since the flow is assumed to be inviscid, all the viscous and heat conduction terms are eliminated. Potential flow methods are thus most valid at high Reynolds numbers. The key assumption, however, is irrotationality. Since $\nabla \times \vec{V} = 0$, the velocity can be expressed as the gradient of a scalar, $\vec{V} = \nabla \phi$. This is because mathematically, $\nabla \times (\nabla \phi)$ is identically equal to zero for any scalar quantity ϕ. In the current context, the scalar ϕ is called the velocity potential. The reason for the last assumption, isentropic flow, will be given in the next section.

4.2 Governing Equations

The irrotationality condition allows the velocity field to be described by a single equation for the velocity potential ϕ. To derive this equation, we start with the continuity equation. Setting $u = \phi_x$ and $v = \phi_y$,

$$\frac{\partial}{\partial x}(\rho \phi_x) + \frac{\partial}{\partial y}(\rho \phi_y) = 0$$

Expanding the derivatives, continuity may be written as

$$\rho(\phi_{xx} + \phi_{yy}) + \phi_x \frac{\partial \rho}{\partial x} + \phi_y \frac{\partial \rho}{\partial y} = 0 \tag{4-6}$$

Using the *x*-momentum and continuity equations we can write

$$\frac{\partial p}{\partial x} = -\rho u \frac{\partial u}{\partial x} - \rho v \frac{\partial u}{\partial y}$$

But $\nabla \times \vec{V} = 0$ gives $\partial u/\partial y = \partial v/\partial x$. Therefore

$$\begin{aligned} \frac{\partial p}{\partial x} &= -\rho u \frac{\partial u}{\partial x} - \rho v \frac{\partial v}{\partial x} \\ &= -\rho \frac{\partial}{\partial x}\left(\frac{u^2 + v^2}{2}\right) \end{aligned} \tag{4-7}$$

Similarly, using the *y*-momentum and continuity equations we can write

$$\frac{\partial p}{\partial y} = -\rho \frac{\partial}{\partial y}\left(\frac{u^2 + v^2}{2}\right) \tag{4-8}$$

Combining equations (4-7) and (4-8), we get

$$\begin{aligned} dp &= -\rho d\left(\frac{u^2 + v^2}{2}\right) \\ &= -\rho d\left(\frac{\phi_x^2 + \phi_y^2}{2}\right) \end{aligned} \tag{4-9}$$

Now, since we assumed isentropic flow, the speed of sound a is defined by $a^2 = dp/d\rho$. Thus

$$d\rho = \frac{dp}{a^2} = -\frac{\rho}{a^2} d\left(\frac{\phi_x^2 + \phi_y^2}{2}\right)$$

Therefore,

$$\frac{\partial \rho}{\partial x} = -\frac{\rho}{a^2}(\phi_x \phi_{xx} + \phi_y \phi_{xy}) \tag{4-10}$$

$$\frac{\partial \rho}{\partial y} = -\frac{\rho}{a^2}(\phi_x \phi_{yx} + \phi_y \phi_{yy}) \tag{4-11}$$

Substituting these expressions into equation (4-6) gives

$$\left(1 - \frac{\phi_x^2}{a^2}\right)\phi_{xx} + \left(1 - \frac{\phi_y^2}{a^2}\right)\phi_{yy} - 2\frac{\phi_x \phi_y}{a^2}\phi_{xy} = 0 \tag{4-12}$$

This equation, which is valid for compressible potential flow, is called the full potential equation. It is a non-linear second-order partial differential equation, and is in non-conservation form. If the speed of sound $a \to \infty$, implying incompressible flow, this equation reduces to Laplace's equation.

$$\phi_{xx} + \phi_{yy} = 0 \tag{4-13}$$

This equation is still second-order, but linear, and therefore easier to solve.

Once the velocity potential ϕ, and hence the velocity field itself, is known, the pressure, temperature, etc., can be computed from the momentum and energy equations.

A few words should be said about the mathematical character of the potential flow equation. (This also applies to the Euler equations to be discussed later). For subsonic flow, the equation is elliptic. This means that the solution at a point depends on the conditions at all the boundaries of the flow domain, including the downstream boundary. For supersonic flow however, the equation is hyperbolic, and the solution at a point depends only on the upstream conditions.

4.3 Solution Methods

For incompressible flows, since the governing equation is linear, complex flows can be described by superposition of solutions for simpler flows. A common procedure is to distribute a series of point sources and sinks, of properly varying strengths, along the surface of the duct. In three dimensions these procedures are called panel methods. The incompressible equation can also be solved using complex variable methods, in which a complex geometry is transformed into a simple geometry using conformal mapping. However, this procedure is limited to two-dimensional flows. There are also several iterative numerical techniques that have been used.

Compressible flows are sometimes computed by solving the incompressible problem and applying a compressibility correction. For slender geometries that only ''slightly'' perturb the uniform external flow, small perturbation methods can be used. This assumption allows the full potential equation to be linearized, and therefore more easily solved.

And finally, the potential flow equations may also be solved using finite difference, finite volume, and finite element methods.

4.4 +'s and –'s

Potential flow methods have been around for many years. The mathematical theory is well understood, and the potential equation is relatively easy to solve, especially for incompressible flow. There are many computer codes available, and they are generally easy to use.

One of the limitations of using potential flow methods for internal flow is that viscous effects are often important and potential flow is, of course, inviscid. The assumption of isentropic flow means that these methods are, strictly speaking, not valid across shock waves. However, if the Mach number normal to the shock is near one the flow is nearly isentropic. In addition, methods that solve the potential equation in non-conservation form, as presented earlier, often have trouble conserving mass (the so-called ''leakage'' problem).

Potential flow methods are most useful in subsonic or transonic flows in which the pressure distribution is of primary interest and in which viscous effects are relatively minor. They are generally cheap to use and are therefore often used in preliminary design studies that require many cases to be run. They also can be used to determine a pressure distribution for boundary layer or parabolized Navier-Stokes analyses. The full potential equation is the basis for many transonic flow analyses.

4.5 Example 1

In the following figure, potential flow results are presented and compared with experimental data for a three-dimensional ''scoop'' inlet. The extended lower lip, or scoop, extends the angle of attack range for the inlet by influencing the incoming flow in such a way as to inhibit flow separation just inside the lower lip. The flow was computed by Kao (1981) using the 3-D incompressible panel method of Hess, Mack, and Stockman (1979). For an arbitrary inlet, this analysis first computes four fundamental solutions — uniform free-stream flow parallel to each of the

three coordinate axes, plus static operation of the inlet. Superposition of these four solutions is used to obtain the final result. Compressibility is modeled using the compressibility correction of Lieblein and Stockman (1972). Approximately 700 panels were used to model the geometry, which included a centerbody and downstream extension not shown in the figure.

The inlet was run at an angle of attack of 50°. The free stream velocity was 41 m/sec, resulting in a throat Mach number of 0.63. The static to total pressure ratio p/p_T is plotted as a function of axial distance at four circumferential locations. The experimental data were taken by Abbott (1977). The agreement between the potential flow results and the experimental data is generally very good. The poorest agreement is along the lower internal surface, and is probably due to boundary blockage effects and possible flow separation. These effects, of course, are not modeled by the potential flow analysis.

4.6 Example 2

The second potential flow example was computed by Reyhner (1982). He studied the transonic flow through a typical turbofan inlet with an asymmetric lip, as shown in the following figure. The tilt of the inlet centerline with respect to the engine centerline is intended to reduce drag by aligning the inlet with the local incoming flow at cruise conditions. Dimensions in the figure are in meters for the full-scale inlet.

Reyhner's method solves the full 3-D potential equation using an iterative successive line over-relaxation (SLOR) finite difference method. The computational grid near the inlet is shown in the figure.

In the next figure, computed and experimental surface Mach numbers are plotted as a function of axial distance at three circumferential locations. The experimental data are unpublished results from a 0.16-scale model test in the Boeing 9×9 foot low speed propulsion wind tunnel. The angle of attack was 20° and the free stream velocity was 90 m/sec.

The agreement is generally very good except along the bottom (windward) surface. As in the previous example, this disagreement is believed due to blockage effects of the thickening boundary layer, which is close to separation, just inside the lower lip. It should be noted that three other cases, with lower peak Mach numbers, were also computed and agreed more closely with experiment.

5. EULER ANALYSES

5.1 Assumptions Made

Like potential flow analyses, Euler analyses are inviscid. However, unlike potential flow analyses, that is the only assumption that is made. The flow can be rotational, non-isentropic, and even unsteady.

The following equations relate the assumptions made for Euler flow to the terms in the Navier-Stokes equations, showing the terms that are eliminated. These equations are written for steady flow, but that is not required.

$$\frac{\partial(\rho u)}{\partial x} + \frac{\partial(\rho v)}{\partial y} = 0 \tag{5-1}$$

$$\frac{\partial(\rho u^2)}{\partial x} + \frac{\partial(\rho uv)}{\partial y} = -\frac{\partial p}{\partial x} + \cancel{\frac{1}{Re_r}\left(\frac{\partial \tau_{xx}}{\partial x} + \frac{\partial \tau_{xy}}{\partial y}\right)} \tag{5-2}$$

$$\frac{\partial(\rho uv)}{\partial x} + \frac{\partial(\rho v^2)}{\partial y} = -\frac{\partial p}{\partial y} + \cancel{\frac{1}{Re_r}\left(\frac{\partial \tau_{xy}}{\partial x} + \frac{\partial \tau_{yy}}{\partial y}\right)} \tag{5-3}$$

$$\frac{\partial(uE_T)}{\partial x} + \frac{\partial(vE_T)}{\partial y} = -\frac{\partial(up)}{\partial x} - \frac{\partial(vp)}{\partial y} - \cancel{\frac{1}{Re_r Pr_r}\left(\frac{\partial q_x}{\partial x} + \frac{\partial q_y}{\partial y}\right)}$$

$$+\cancel{\frac{1}{Re_r}\left[\frac{\partial}{\partial x}(u\tau_{xx} + v\tau_{xy}) + \frac{\partial}{\partial y}(u\tau_{xy} + v\tau_{yy})\right]} \tag{5-4}$$

5.2 Governing Equations

The Euler equations are thus simply the Navier-Stokes equations with all the viscous and heat conduction terms eliminated. For steady flow, the resulting equations are:

$$\frac{\partial(\rho u)}{\partial x} + \frac{\partial(\rho v)}{\partial y} = 0 \tag{5-5}$$

$$\frac{\partial(\rho u^2)}{\partial x} + \frac{\partial(\rho uv)}{\partial y} = -\frac{\partial p}{\partial x} \tag{5-6}$$

$$\frac{\partial(\rho uv)}{\partial x} + \frac{\partial(\rho v^2)}{\partial y} = -\frac{\partial p}{\partial y} \tag{5-7}$$

$$\frac{\partial(uE_T)}{\partial x} + \frac{\partial(vE_T)}{\partial y} = -\frac{\partial(up)}{\partial x} - \frac{\partial(vp)}{\partial y} \tag{5-8}$$

As in potential flow, these equations are therefore most valid at high Reynolds numbers. Like the Navier-Stokes equations, the Euler equations are a set of coupled nonlinear partial differential equations, but first-order instead of second-order. For steady flow, their mathematical character is the same as the potential equation — elliptic in space for subsonic flow and hyperbolic in space for supersonic flow. For unsteady flow they are hyperbolic in time.

5.3 Solution Methods

The Euler equations are most commonly solved using finite difference techniques. For supersonic flow, the equations are hyperbolic in space and can be solved by forward marching in the streamwise direction. For subsonic flow they are elliptic in space, but hyperbolic in time. Steady subsonic (or even supersonic) flows are therefore often solved by marching the unsteady equations in time until a steady state is reached. Both explicit and implicit methods have been used. The trend seems to be toward implicit methods. If only the steady-state solution is of interest, various techniques are often used to accelerate convergence, and the results may not be time-accurate. Some researchers are using multi-grid techniques, in which a series of grids from coarse to fine are used to speed convergence to steady state. Finite volume and finite element methods have also been used.

The method of characteristics is the most nearly exact method for numerically solving hyperbolic partial differential equations. It can be used to solve the Euler equations for steady supersonic flow, or unsteady subsonic or supersonic flow. With this method the partial differential equations reduce to ordinary differential equations along characteristic directions. The trend today, however, seems to be toward the more easily implemented finite difference methods.

5.4 +'s and −'s

The Euler equations include rotational effects. For instance, if the flow entering a duct has a boundary layer-like profile, secondary flow development and even flow separation can be computed with the Euler equations. They are also valid across shock waves. With finite difference methods, shock waves are generally ''captured'' by the solution and smeared over a few grid points. Some form of smoothing, or artificial viscosity, is usually required for stability or to eliminate oscillations. Because the flow is inviscid, there are no shear layers with large gradients to resolve and therefore fewer grid points are needed than for a Navier-Stokes solution.

For many internal flows, however, viscous effects are important and their omission may be a limitation. These codes can also be difficult to run because of the need to select time step size to optimize convergence, parameters controlling artificial viscosity, etc. Time dependent methods can be long running, although still faster than Navier-Stokes methods because fewer grid points are needed.

Like potential flow analyses, Euler analyses are most useful for flows in which the pressure distribution is of primary interest and in which viscous effects are relatively minor. They can be used to investigate candidate designs of propulsion system components, and to compute a pressure distribution for use by a boundary layer or parabolized Navier-Stokes analysis.

5.5 Example

The following figure shows Mach number contours for an oblique shock wave reflecting off a flat plate. The free stream Mach number was 2.4, and the shock was generated by a 10° wedge.

These results were computed using Proteus, a user-oriented Navier-Stokes code developed at NASA Lewis, run in Euler mode (Towne, Schwab, and Bui, 1993a,b). With this code, the unsteady governing equations are solved by marching in time using an implicit finite difference technique. Artificial viscosity terms were used to minimize the odd-even decoupling resulting from the use of central differencing, and to control pre- and post-shock oscillations. A 51×51 grid was used, equally spaced in both directions, and convergence to steady state was obtained in about 400 time steps.

Since Euler methods are rotational and non-isentropic, the Rankine-Hugoniot relations are satisfied across the shock waves. Note, however, that the shocks are not sharp discontinuities but are smeared over a few grid points. They could be sharpened by using more grid points, or by packing grid points more tightly in the location of the shocks. It should also be noted that because Euler methods are inviscid, no boundary layer buildup occurs on the flat plate. The actual flow, with a shock - boundary layer interaction, would look quite different near the surface of the plate.

6. BOUNDARY LAYER ANALYSES

6.1 Assumptions Made

Potential flow and Euler analyses are inviscid. At high Reynolds numbers these analyses can yield good results for pressure distributions, but they cannot predict viscous or heat transfer effects. This limits their usefulness for internal flows, where these effects are usually important.

The oldest generalized methods to include these effects are called boundary layer methods, first developed by Prandtl in 1904. He noted that in many applications at high Reynolds numbers, viscous effects are confined to a relatively thin region near solid boundaries called the boundary layer. In deriving the boundary layer equations, the thickness of this region is assumed small relative to the size of the geometry being analyzed, and is said to be of $O(\delta)$. The density, temperature, streamwise velocity, and total enthalpy, along with derivatives in the streamwise direction, are assumed to be of $O(1)$. Gradients normal to the surface are expected to be much larger than gradients along the surface, and are therefore assumed to be of of $O(1/\delta)$. And, since the Reynolds number must be high for the boundary layer approximation to be valid, Re is assumed to be of $O(1/\delta^2)$. These assumed orders of magnitude are to be applied to each term in the fundamental Navier-Stokes equations, and terms of $O(1)$ are to be retained. For simplicity we will restrict the order of magnitude analysis to steady flow.

In the fundamental continuity equation, $\partial(\rho u)/\partial x = O(1)$. This implies that $\partial(\rho v)/\partial y$ must also be $O(1)$, and therefore $v = O(\delta)$.

In the x-momentum equation, then, $\partial(\rho u^2)/\partial x$ and $\partial(\rho uv)/\partial y$ are both $O(1)$. Since the viscous terms must approach zero at the edge of the boundary layer, $\partial p/\partial x$ must also be $O(1)$. Examining the shear stress definitions, it can be seen that $\tau_{xx} = O(1)$, while τ_{xy} is made up of an $O(\delta)$ and an $O(1/\delta)$ term. Therefore,

$$\frac{1}{Re_r}\frac{\partial \tau_{xx}}{\partial x} = O(\delta^2)$$

$$\frac{1}{Re_r}\frac{\partial \tau_{xy}}{\partial y} = O(\delta^2) + O(1)$$

In the y-momentum equation, $\partial(\rho uv)/\partial x$ and $\partial(\rho v^2)/\partial y$ are both $O(\delta)$. Again examining the shear stress definitions, it can be seen that $\tau_{yy} = O(1)$. Therefore,

$$\frac{1}{Re_r}\frac{\partial \tau_{xy}}{\partial x} = O(\delta^3) + O(\delta)$$

$$\frac{1}{Re_r}\frac{\partial \tau_{yy}}{\partial y} = O(\delta)$$

The $\partial p/\partial y$ term is the only one left to be examined in the y-momentum equation. Since the largest of the other terms in the equation is $O(\delta)$, $\partial p/\partial y$ must be at most $O(\delta)$.

In the total enthalpy form of the energy equation, both $\partial(\rho uH)/\partial x$ and $\partial(\rho vH)/\partial y$ are $O(1)$. Note that the v term in the definition of H may be eliminated. The heat flux $q_x = O(1)$ and $q_y = O(1/\delta)$. Therefore,

$$\frac{1}{Re_r Pr_r}\frac{\partial q_x}{\partial x} = O(\delta^2)$$

$$\frac{1}{Re_r Pr_r}\frac{\partial q_y}{\partial y} = O(1)$$

Examining the shear stress terms in the energy equation, we get

$$\frac{1}{Re_r}\frac{\partial(u\tau_{xx})}{\partial x} = O(\delta^2)$$

$$\frac{1}{Re_r}\frac{\partial(v\tau_{xy})}{\partial x} = O(\delta^4) + O(\delta^2)$$

$$\frac{1}{Re_r}\frac{\partial(u\tau_{xy})}{\partial y} = O(\delta^2) + O(1)$$

$$\frac{1}{Re_r}\frac{\partial(v\tau_{yy})}{\partial y} = O(\delta^2)$$

The following equations summarize which terms in the fundamental equations are eliminated in deriving the boundary layer equations.

$$\frac{\partial(\rho u)}{\partial x} + \frac{\partial(\rho v)}{\partial y} = 0 \tag{6-1}$$

$$\frac{\partial(\rho u^2)}{\partial x} + \frac{\partial(\rho uv)}{\partial y} = -\frac{\partial p}{\partial x} + \frac{1}{Re_r}\left(\cancel{\frac{\partial \tau_{xx}}{\partial x}} + \frac{\partial \tau_{xy}}{\partial y}\right) \tag{6-2}$$

$$\cancel{\frac{\partial(\rho uv)}{\partial x}} + \cancel{\frac{\partial(\rho v^2)}{\partial y}} = -\cancel{\frac{\partial p}{\partial y}} + \cancel{\frac{1}{Re_r}}\left(\frac{\partial \tau_{xy}}{\partial x} + \cancel{\frac{\partial \tau_{yy}}{\partial y}}\right) \tag{6-3}$$

$$\frac{\partial(\rho uH)}{\partial x} + \frac{\partial(\rho vH)}{\partial y} = -\frac{1}{Re_r Pr_r}\left(\cancel{\frac{\partial q_x}{\partial x}} + \frac{\partial q_y}{\partial y}\right) + \frac{1}{Re_r}\left[\cancel{\frac{\partial}{\partial x}(u\tau_{xx} + v\tau_{xy})} + \frac{\partial}{\partial y}(u\tau_{xy} + \cancel{v\tau_{yy}})\right] \tag{6-4}$$

With the boundary layer assumptions, the shear stress τ_{xy} and heat flux q_y are given by

$$\tau_{xy} = \mu\left(\cancel{\frac{\partial v}{\partial x}} + \frac{\partial u}{\partial y}\right) \tag{6-5}$$

$$q_y = -k\frac{\partial T}{\partial y} \tag{6-6}$$

Pressure is usually defined by the perfect gas equation of state,

$$p = \rho RT \tag{6-7}$$

The definition of total enthalpy becomes

$$H = c_p T + \frac{1}{2}(u^2 + \cancel{v^2}) \tag{6-8}$$

In the boundary layer equations, all second derivatives in the *x*, or streamwise, direction are eliminated, as are mixed second derivatives. Second derivatives in the *y*, or cross-flow, direction are retained. In addition, the entire cross-flow momentum equation is eliminated.

6.2 Governing Equations

The resulting boundary layer equations, with the viscous and heat conduction terms expanded, are as follows:

$$\frac{\partial(\rho u)}{\partial x} + \frac{\partial(\rho v)}{\partial y} = 0 \tag{6-9}$$

$$\frac{\partial(\rho u^2)}{\partial x} + \frac{\partial(\rho uv)}{\partial y} = -\frac{dp_e}{dx} + \frac{1}{Re_r}\frac{\partial}{\partial y}\left(\mu\frac{\partial u}{\partial y}\right) \tag{6-10}$$

$$\frac{\partial(\rho uH)}{\partial x} + \frac{\partial(\rho vH)}{\partial y} = -\frac{1}{Re_r Pr_r}\frac{\partial}{\partial y}\left(k\frac{\partial T}{\partial y}\right) + \frac{1}{Re_r}\frac{\partial}{\partial y}\left(\mu u\frac{\partial u}{\partial y}\right) \tag{6-11}$$

Note that the pressure gradient term is written as an ordinary derivative, since with the boundary layer approximation, $\partial p/\partial y = 0$. The pressure $p_e(x)$ is generally assumed to be known, typically from a potential flow or Euler analysis, or from experiment. In some internal flow applications, the pressure is computed as part of the boundary layer solution using conservation of total mass flow rate as a basis. The boundary layer equations are parabolic in the streamwise direction, and can therefore be solved by forward marching in x.

6.3 Solution Methods

The earliest solution methods developed for the boundary layer equations were integral methods. Many different integral methods have been proposed. Typically, they are derived by assuming a functional form for the velocity profile, for instance a power law like $u/u_e = (y/\delta)^{1/7}$, plugging it into the x-momentum equation, and analytically integrating over y. The result is an ordinary differential equation, or in some cases equations, in x for some boundary layer parameter such as displacement thickness, momentum thickness, etc.

Most of the more recent boundary layer methods solve the partial differential boundary layer equations themselves, by forward marching in the streamwise direction using explicit or implicit finite difference, finite volume, or finite element techniques.

6.4 +'s and –'s

Boundary layer methods are the simplest methods that can be used that include viscous and heat transfer effects. Like potential flow methods, they have been around for a long time. Working computer codes are widely available, and they are generally fairly fast and easy to use.

Although the boundary layer equations include viscous effects, the streamwise viscous diffusion terms have been eliminated. This restricts them to attached flow, so that the streamwise velocity is always positive. There are, however, various numerical approximations like the "FLARE" approximation (Reyhner and Flugge-Lotz, 1968) that allow the equations to be marched through small regions of separated flow. Boundary layer methods are valid only for thin shear layers, and cannot be used to compute completely viscous internal flows. Another limitation is the need for a known pressure distribution, requiring an initial potential flow or Euler analysis.

Boundary layer methods are most useful in high Reynolds number flows with thin viscous regions, where the boundary layer has negligible effect on the pressure field. They are generally cheap to use and are therefore often used in preliminary design studies that require many cases to be run. They are sometimes used in conjunction with a potential flow or Euler analysis in an interactive mode. In these cases, typically, the inviscid analysis is used to get an initial pressure distribution, the boundary layer analysis is used to get a displacement thickness distribution, a new "effective" body shape is determined, the inviscid analysis is rerun, etc.

6.5 Example 1

As an example of a boundary layer analysis for internal flow, the method of Vadyak, Hoffman, and Bishop (1984) for flow through supersonic inlets will be used. The following figure is a schematic of a typical mixed-compression supersonic inlet. Turbulent boundary layers develop along both the cowl and centerbody. Since there are shock waves in the inlet, shock - boundary layer interactions occur. Vadyak, et. al., used a second-order method

of characteristics algorithm with discrete shock wave fitting to compute the inviscid flow through the inlet. The boundary layer was then computed using a second-order implicit finite difference technique. Turbulence was modeled by the two-layer eddy viscosity model of Cebeci, Kaups, Mosinskis, and Rehn (1973). An integral control volume analysis was used for the shock - boundary layer interactions.

The analysis was applied to a Boeing Mach 3.5 mixed-compression axisymmetric inlet. In this inlet, the centerbody is translated forward at off-design (lower) Mach numbers in order to maintain supersonic flow through the throat. The amount of translation is given by the value of $\Delta x/R_c$, where R_c is the cowl lip radius.

In the next figure, computed total pressure profiles are compared with experimental data (Syberg and Koncsek, 1975; Koncsek, 1975). Profiles are presented on the cowl and centerbody at the axial stations specified are presented for off-design free stream Mach numbers of 2.1 and 2.3. The effect of viscosity is obvious in the total pressure loss through the boundary layer as the wall is approached. The boundary layer is thicker on the centerbody than the cowl because of its longer development length.

6.6 Example 2

Results from a coupled Euler/boundary layer analysis for a three-dimensional transonic fan rotor are shown in the following figure. The calculations were done by Pierzga and Wood (1985), using the Euler code developed by Denton (1982), and later modified by Denton (1983) to include a simple boundary layer correction procedure. The Euler equations were solved by marching in time using a finite-volume technique. A multi-grid procedure was used to speed convergence. The computational grid consisted of 21 points from blade to blade, 95 points in the streamwise direction (50 on the blade, 45 upstream and downstream), and 11 points from hub to shroud. The effect of the boundary layers was modeled by allowing flow to pass through the walls at a rate proportional to the boundary layer displacement thickness. This displacement thickness was computed from the von Karman integral boundary layer equation, with a constant shape factor of 1.5 and a constant skin friction coefficient of 0.005. Depending on the flow conditions, the calculation required 1300 to 2486 time steps, corresponding to 9 to 17 minutes of CPU time on a Cray-1 computer.

In the figure computed Mach number contours are shown at the 10 per cent span location, measured from the rotor tip, for three slightly different cases. For all cases the inlet Mach number at the rotor tip was approximately 1.38. In case 1, the code was run without the boundary layer correction. The flow accelerates slightly through the blade passage, with a normal shock at the exit. The shock, of course, is smeared over a few grid points by the numerical procedure. In case 3, the flow was recomputed with the boundary layer correction added. One effect of the boundary layer is to decrease the effective flow area, causing the normal shock position to shift upstream. Note, however, that it also reduces the mass flow through the passage. In case 2, the code was again run without the boundary layer correction, but with the back pressure artificially raised to a level that yields the same mass flow as in case 3. This also caused the normal shock position to shift upstream, to approximately the same position as in case 3.

7. PARABOLIZED NAVIER-STOKES ANALYSES

7.1 Assumptions Made

There are many cases where viscous effects are important, but boundary layer methods are not sufficient. Examples include diffusing internal flows in which boundary layers on opposite walls merge, so that there is no inviscid region, and corner flows, where viscous derivatives in two directions are important. The Navier-Stokes equations could of course be solved for these flows, but they are expensive and often difficult to solve.

Fortunately, for many cases there is an alternative. A reduced set of equations can be derived that are easier to solve than the Navier-Stokes equations, but contain more physics than the boundary layer equations. These are the so-called ''parabolized'' Navier-Stokes, or PNS, equations, and they are becoming more and more popular. They apply throughout the flow field, which is not split into inviscid and viscous regions. ''Parabolized'' is actually bad terminology, but it has caught on. The steady flow equations are actually of mixed hyperbolic-parabolic type. The key point, however, is that they can be solved by forward marching in the streamwise direction.

The derivation of the PNS equations is not as rigorous as the boundary layer equations, and several different versions appear in the literature. With some exceptions, the derivation is roughly equivalent to keeping both the $O(1)$ and $O(\delta)$ terms in the order of magnitude analysis used in deriving the boundary layer equations. All methods neglect second derivatives in the streamwise direction. In addition, special treatment is required for the pressure gradient term in the streamwise momentum equation. (More on this later.)

The following equations indicate which terms in the fundamental equations are eliminated in deriving one version of the PNS equations.

$$\frac{\partial(\rho u)}{\partial x} + \frac{\partial(\rho v)}{\partial y} = 0 \tag{7-1}$$

$$\frac{\partial(\rho u^2)}{\partial x} + \frac{\partial(\rho uv)}{\partial y} = -\frac{\partial p}{\partial x} + \frac{1}{Re_r}\left(\cancel{\frac{\partial \tau_{xx}}{\partial x}} + \frac{\partial \tau_{xy}}{\partial y}\right) \tag{7-2}$$

$$\frac{\partial(\rho uv)}{\partial x} + \frac{\partial(\rho v^2)}{\partial y} = -\frac{\partial p}{\partial y} + \frac{1}{Re_r}\left(\cancel{\frac{\partial \tau_{xy}}{\partial x}} + \frac{\partial \tau_{yy}}{\partial y}\right) \tag{7-3}$$

$$\frac{\partial(\rho uH)}{\partial x} + \frac{\partial(\rho vH)}{\partial y} = -\frac{1}{Re_r Pr_r}\left(\cancel{\frac{\partial q_x}{\partial x}} + \frac{\partial q_y}{\partial y}\right) + \frac{1}{Re_r}\left[\cancel{\frac{\partial}{\partial x}(u\tau_{xx} + v\tau_{xy})} + \frac{\partial}{\partial y}(u\tau_{xy} + v\tau_{yy})\right] \tag{7-4}$$

With the PNS assumptions, the shear stresses τ_{xy} and τ_{yy}, and the heat flux q_y, are given by

$$\tau_{xy} = \mu\left(\cancel{\frac{\partial v}{\partial x}} + \frac{\partial u}{\partial y}\right) \tag{7-5}$$

$$\tau_{yy} = 2\mu\frac{\partial v}{\partial y} + \lambda\left(\cancel{\frac{\partial u}{\partial x}} + \frac{\partial v}{\partial y}\right) \tag{7-6}$$

$$q_y = -k\frac{\partial T}{\partial y} \tag{7-7}$$

Pressure is again usually defined by the perfect gas equation of state,

$$p = \rho RT \tag{7-8}$$

And the definition of total enthalpy is

$$H = c_p T + \frac{1}{2}(u^2 + v^2) \tag{7-9}$$

In the PNS equations, derivatives in the streamwise direction in the viscous and heat conduction terms are eliminated. Note that, unlike in the boundary layer equations, the cross-flow momentum equation is retained in the PNS equations.

7.2 Governing Equations

The resulting PNS equations, with the viscous and heat conduction terms expanded, are as follows:

$$\frac{\partial(\rho u)}{\partial x} + \frac{\partial(\rho v)}{\partial y} = 0 \tag{7-10}$$

$$\frac{\partial(\rho u^2)}{\partial x} + \frac{\partial(\rho uv)}{\partial y} = -\frac{\partial p}{\partial x} + \frac{1}{Re_r}\frac{\partial}{\partial y}\left(\mu \frac{\partial u}{\partial y}\right) \tag{7-11}$$

$$\frac{\partial(\rho uv)}{\partial x} + \frac{\partial(\rho v^2)}{\partial y} = -\frac{\partial p}{\partial y} + \frac{1}{Re_r}\frac{\partial}{\partial y}\left[(2\mu + \lambda)\frac{\partial u}{\partial y}\right] \tag{7-12}$$

$$\frac{\partial(\rho uH)}{\partial x} + \frac{\partial(\rho vH)}{\partial y} = -\frac{1}{Re_r Pr_r}\frac{\partial}{\partial y}\left(k\frac{\partial T}{\partial y}\right) + \frac{1}{Re_r}\frac{\partial}{\partial y}\left[\mu u\frac{\partial u}{\partial y} + (2\mu + \lambda)v\frac{\partial v}{\partial y}\right] \tag{7-13}$$

Except for the pressure gradient term in the x-momentum equation, the PNS equations are of mixed hyperbolic-parabolic type in the x, or streamwise, direction, and could be solved by forward marching in x. However, the $\partial p/\partial x$ term allows information to propagate upstream in subsonic flow. Note that this situation occurs not only in completely subsonic flow, but also in the subsonic region near the wall in primarily supersonic flow. This makes a streamwise marching procedure ill-posed. Without special treatment of the streamwise pressure gradient, exponentially growing solutions called branching solutions can occur. Various procedures have been used to eliminate this problem and allow a streamwise marching solution procedure to be used. The way the streamwise pressure gradient is treated is often what distinguishes one PNS method from another.

For primarily supersonic flow, with embedded subsonic regions, one procedure that has been used is to either neglect $\partial p/\partial x$, or to specify it as in a boundary layer analysis and treat it as a source term. In general, though, $\partial p/\partial x$ is not negligible, or known a priori. Another solution is to simply lag the $\partial p/\partial x$ term, evaluating it from the previous marching step. However, this leads to an undesirable restriction on the minimum marching step size that may be taken. Another procedure that has been used is to set the pressure in the subsonic region equal to its value at the first supersonic location for each x marching station. Under some conditions, however, this still allows branching solutions to occur. A somewhat different procedure, for flows with thin subsonic regions near walls, is to use approximate forms of the continuity and y-momentum equations in the subsonic region. This has been shown to suppress branching solutions without any special treatment of the $\partial p/\partial x$ term.

For fully subsonic flow, p in the x-momentum equation is typically treated as a function of x only, and computed iteratively using conservation of total mass flow as a basis. An improvement on this is to let $p(x, y) = p'(x) + P(x, y)$ in the x-momentum equation, where $P(x, y)$ is a known estimate for the pressure field, from a potential flow solution for example, and $p'(x)$ is computed during the marching solution.

So-called ‘‘partially parabolized’’ methods, in which an initial known two-dimensional pressure field is updated iteratively using multiple streamwise marching sweeps, have been used for both primarily supersonic and

fully subsonic flow.

As presented here, the PNS equations are for two-dimensional flow. However, PNS analyses are also used, perhaps even more often, for three-dimensional flow.

7.3 Solution Methods

In solving the PNS equations, finite difference methods dominate, although finite volume and finite element methods have also been used. As mentioned previously for Euler analyses, the trend is towards the use of implicit instead of explicit methods.

7.4 +'s and −'s

Since the PNS equations include the cross-flow momentum equations, and retain viscous derivatives in both cross-flow directions (in 3-D), they apply to flow situations that boundary layer methods can't handle. They are used throughout the flow field, so a separate inviscid solution may not be needed. And, since the equations are solved by spatial marching, PNS methods are faster and use less storage than Navier-Stokes methods.

As in boundary layer analyses, however, neglecting the streamwise viscous diffusion terms means the flow must remain attached, except for small separation bubbles that can be computed using the ''FLARE'' approximation. A final problem with PNS methods is that they are still somewhat ''researchy'' and can be difficult to use, especially for complex geometries.

PNS methods are most applicable to relatively high Reynolds number flows without reverse flow. They are at the stage where they can be used in design, but are generally used more for verification and problem investigation than for large parametric studies.

7.5 Example 1

This example will show results from PEPSIG, a three-dimensional parabolized Navier-Stokes analysis for subsonic flow (Briley and McDonald, 1979; Levy, McDonald, Briley, and Kreskovsky, 1980; Levy, Briley, and McDonald, 1983). In this analysis, the pressure in the streamwise momentum equation is represented as $p(x, y, z) = p'(x) + P(x, y, z)$, where $P(x, y, z)$ is computed from a three-dimensional potential flow analysis, and $p'(x)$ is computed during the marching solution using conservation of total mass flow as a basis. The computations were done by Towne and Flitcroft as part of a joint NASA/RAE research program on intake duct flows (Towne and Flitcroft, 1986).

Calculations were made for flow through two generic S-shaped intake ducts with offset/length ratios of 0.30 and 0.45, as shown in the following figure. Each intake duct had a circular cross-section, and an area ratio of 1.4. Inlet Mach numbers ranged from 0.395 to 0.794, and Reynolds numbers from 3.9×10^6 to 6.6×10^6, based on the inlet diameter and flow conditions. The flow was turbulent, modeled using the model of McDonald and Camarata (1969).

In the next figure, the development of pressure-driven secondary flow is shown for the 0.45 offset S-duct. Computed secondary velocity vectors (i.e., the velocity in planes normal to the duct centerline) are presented at three streamwise stations. In the first bend, the high pressure at the outside (top) of the bend drives the low energy boundary layer toward the inside (bottom) of the bend, while the core flow responds to centrifugal effects and moves toward the outside (top) of the bend. The result is a pair of counter-rotating secondary flow vortices in the lower half of the cross-section.

In the second bend, the direction of the cross-flow pressure gradients reverses. The pressure is now higher in the bottom half of the cross-section. However, the flow enters the second bend with a vortex pattern already established. The net effect is to tighten and concentrate the existing vortices near the bottom of the duct, in agreement with classical secondary flow theory.

These secondary flows cause a significant amount of flow distortion. In the next figure, contours of constant streamwise velocity (i.e., the velocity in the direction of the duct centerline) are shown at several stations for the 0.30 offset S-duct. As the flow enters the first bend, the boundary layer at the top of the duct initially thickens due to the locally adverse pressure gradient in that region. The effects of the secondary flow soon dominate, however, and by the end of the duct most of the low-energy flow has moved to the bottom of the duct. The horseshoe-shaped

distortion pattern at the exit is typical of S-bend flows.

In the final figure, computed total pressure contours at the exit of the 0.30 offset S-duct are compared with experimental data of Willmer, Brown, and Goldsmith (1981) for the same duct. It should be noted that a compressor face hub was present in the actual duct, but was not modeled in the computations. Despite this, the agreement between the computational and experimental results is generally very good. This case was run using a 50×50 mesh in the cross-plane, packed near the wall to resolve the boundary layer, with 67 evenly spaced streamwise marching stations. Seven minutes of CPU time were required on a Cray X-MP computer.

7.6 Example 2

In the following figure, computed results are presented from PEPSIS, a three-dimensional parabolized Navier-Stokes analysis for primarily supersonic flow (Buggeln, McDonald, Kreskovsky, and Levy, 1979; Buggeln, McDonald, and Kim, 1983). In this analysis, branching solutions are suppressed by using approximate forms of the continuity and y-momentum equations in the subsonic region. No special treatment was required for the $\partial p/\partial x$ term in the streamwise momentum equation. The computations were done by Anderson and Benson (1983).

The problem is a three-dimensional sidewall shock - boundary layer interaction. Complex flows like this can occur in ''two-dimensional'' mixed-compression supersonic inlets when the oblique shock generated by the ramp interacts with the sidewall boundary layer. In this problem, the shock was generated by a 10° wedge mounted in a wind tunnel, flush with the sidewall. The incoming Mach number was 2.94, and the Reynolds number was 1.28×10^6, based on a reference length of 0.667 ft. The flow was turbulent, computed using the model of McDonald and Camarata (1968).

Shown in the figure are the secondary velocity vectors (i.e., the velocity vectors in the cross-flow directions, without the streamwise component) at selected streamwise stations. The shock position as it cuts through the cross-plane is indicated by the change in direction of the secondary velocity vectors. The high pressure downstream of the shock (which is the region nearest the wedge surface) forces the low-energy boundary layer flow to migrate upward along the sidewall. The flow on the wedge is then drawn in toward the sidewall and the flow moving up the sidewall turns over, forming a complex secondary flow vortex in the corner. The low energy flow thus accumulates in the corner region, and is probably the cause of the high heating rates detected experimentally (Oskam, Vas, and Bogdonoff, 1976). This case was run using a 40×60 mesh in the cross-plane, packed near the walls to resolve the boundary layers, with 90 streamwise marching stations. The calculation required 36 minutes of CPU time on an IBM 370/3033 computer.

8. TIME-AVERAGED NAVIER-STOKES ANALYSES

8.1 Governing Equations

The time-averaged Navier-Stokes equations are

$$\frac{\partial \rho}{\partial t} + \frac{\partial (\rho u)}{\partial x} + \frac{\partial (\rho v)}{\partial y} = 0 \tag{8-1}$$

$$\frac{\partial (\rho u)}{\partial t} + \frac{\partial (\rho u^2)}{\partial x} + \frac{\partial (\rho uv)}{\partial y} = -\frac{\partial p}{\partial x} + \frac{1}{Re_r}\left(\frac{\partial \tau_{xx}}{\partial x} + \frac{\partial \tau_{xy}}{\partial y}\right) \tag{8-2}$$

$$\frac{\partial (\rho v)}{\partial t} + \frac{\partial (\rho uv)}{\partial x} + \frac{\partial (\rho v^2)}{\partial y} = -\frac{\partial p}{\partial y} + \frac{1}{Re_r}\left(\frac{\partial \tau_{xy}}{\partial x} + \frac{\partial \tau_{yy}}{\partial y}\right) \tag{8-3}$$

$$\frac{\partial (E_T)}{\partial t} + \frac{\partial (uE_T)}{\partial x} + \frac{\partial (vE_T)}{\partial y} = -\frac{\partial (up)}{\partial x} - \frac{\partial (vp)}{\partial y} - \frac{1}{Re_r Pr_r}\left(\frac{\partial q_x}{\partial x} + \frac{\partial q_y}{\partial y}\right) + \frac{1}{Re_r}\left[\frac{\partial}{\partial x}(u\tau_{xx} + v\tau_{xy}) + \frac{\partial}{\partial y}(u\tau_{xy} + v\tau_{yy})\right] \tag{8-4}$$

The shear stresses and heat fluxes are given by

$$\tau_{xx} = 2\mu \frac{\partial u}{\partial x} + \lambda\left(\frac{\partial u}{\partial x} + \frac{\partial v}{\partial y}\right) \tag{8-5}$$

$$\tau_{yy} = 2\mu \frac{\partial v}{\partial y} + \lambda\left(\frac{\partial u}{\partial x} + \frac{\partial v}{\partial y}\right) \tag{8-6}$$

$$\tau_{xy} = \mu\left(\frac{\partial u}{\partial y} + \frac{\partial v}{\partial x}\right) \tag{8-7}$$

$$q_x = -k \frac{\partial T}{\partial x} \tag{8-8}$$

$$q_y = -k \frac{\partial T}{\partial y} \tag{8-9}$$

Pressure is again usually defined by the perfect gas equation of state,

$$p = \rho RT \tag{8-10}$$

And the total energy is defined as

$$E_T = \rho c_v T + \frac{1}{2}\rho(u^2 + v^2) \tag{8-11}$$

The above equations are the same as the fundamental equations shown at the beginning of this presentation. The term ‘‘time-averaged’’ refers to the procedure used to develop equations for turbulent flow that can be solved for practical problems with today’s computer systems. They can still be used for unsteady turbulent flow, as long as the

time scale of the unsteadiness is long compared to the time scale of the turbulent fluctuations.

For laminar flow, the only assumptions made in deriving the governing differential equations are that the fluid is Newtonian, that it can be treated as a continuum, and that body forces and internal heat addition are negligible. For turbulent flow the only additional assumption, and depending on the complexity of the flow it could be a big one, is in the choice of turbulence model. Of course, further assumptions are usually made in choosing an equation of state. Typically, a perfect gas is assumed.

For unsteady flow, the Navier-Stokes equations are of mixed hyperbolic-parabolic type.

8.2 Solution Methods

The Navier-Stokes equations are usually solved by marching in time. Finite difference methods are the most common, although finite volume and finite element methods have also been used. Both explicit and implicit methods have been used, with the trend today toward implicit methods. As with the unsteady Euler equations, if only the steady state solution is of interest, acceleration techniques are often used to speed convergence, and the results may not be time accurate.

8.3 +'s and −'s

Except for the need to model instead of actually compute turbulence, the Navier-Stokes equations are the most complete mathematical model possible for the continuum flow of a Newtonian fluid. No other assumptions or approximations are built into the governing equations. However, various assumptions, such as a perfect gas law, are often used in the auxiliary equations.

Unfortunately, using a Navier-Stokes method is expensive. They require large amounts of computer time and memory. They are also newer and less mature than simpler methods. Developing and/or using a Navier-Stokes analysis is not necessarily straightforward, and is basically still a research area itself.

The Navier-Stokes equations can be applied to any type of flow. The expense and difficulty involved in using them currently limits their practical application. They can be used in design problems where the potential payoff is high enough to offset their cost, and in research into complex flow physics problems.

8.4 Example 1

In this example, transonic turbulent flow was computed in a converging-diverging duct. The calculations were made using Proteus, a user-oriented Navier-Stokes code being developed at NASA Lewis (Towne, Schwab, and Bui, 1993a,b). Turbulence was modeled using the eddy viscosity model of Baldwin and Lomax (1978). The flow entered the duct subsonically, accelerated through the throat to supersonic speed, then decelerated through a normal shock and exited the duct subsonically.

The initial conditions were simply zero velocity and constant pressure and temperature. Thus, $u = v = 0$ and $p = T = 1$ everywhere in the flow field.

This calculation was performed in three separate runs. In the first run, the exit static pressure was gradually lowered to a value low enough to establish supersonic flow throughout the diverging portion of the duct. The pressure was lowered as follows:

$$p(t) = \begin{cases} 0.99 & \text{for } 1 < n \le 100 \\ -2.1405 \times 10^{-3} n + 1.20405 & \text{for } 101 \le n \le 500 \\ 0.1338 & \text{for } 501 \le n \le 3001 \end{cases}$$

where n is the time level. The equation for p for $101 \le n \le 500$ is simply a linear interpolation between $p = 0.99$ and $p = 0.1338$. In the second run, the exit pressure was gradually raised to a value consistent with the formation of a normal shock just downstream of the throat. Thus,

$$p(t) = \begin{cases} 3.4327 \times 10^{-4} n - 0.89636 & \text{for } 3001 < n \le 5000 \\ 0.82 & \text{for } 5001 \le n \le 6001 \end{cases}$$

Again, the equation for p for $3001 < n \le 5000$ is simply a linear interpolation between $p = 0.1338$ and $p = 0.82$. In the third run, the exit pressure was kept constant at 0.82.

The remaining boundary conditions were the same for all runs. At the inlet, constant total pressure and temperature were specified, and the y-velocity and the normal gradient of the x-velocity were both set equal to zero. At the exit, the normal gradients of temperature and both velocity components were set equal to zero. At both walls, no-slip adiabatic conditions were used, and the normal pressure gradient was set equal to zero.

The computed flow field is shown in the following figure in the form of constant Mach number contours. Contours are plotted at Mach numbers ranging from 0.0 to 1.2 in increments of 0.1.

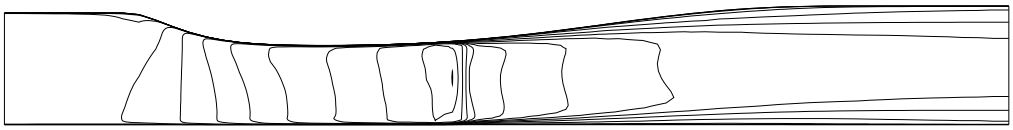

Computed Mach number contours for transonic diffuser flow.

The flow enters the duct at about $M = 0.46$, accelerates to just under $M = 1.3$ slightly downstream of the throat, shocks down to about $M = 0.78$, then decelerates and leaves the duct at about $M = 0.51$. The normal shock in the throat region and the growing boundary layers in the diverging section can be seen clearly. Because this is a shock capturing analysis, the normal shock is smeared in the streamwise direction.

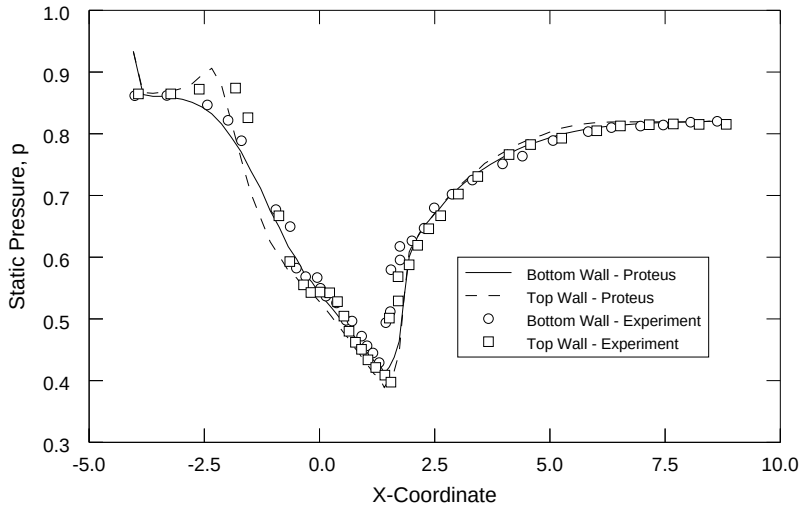

Computed and experimental static pressure distribution for transonic diffuser flow

The computed distribution of the static pressure ratio along the top and bottom walls is compared with experimental data (Hsieh, Wardlaw, Collins, and Coakley, 1987) in the above figure. The static pressure ratio is here defined as $p/(p_T)_0$, where $(p_T)_0$ is the inlet core total pressure. The computed results generally agree well with the experimental data, including the jump conditions across the normal shock. The predicted shock position, however, is slightly downstream of the experimentally measured position, probably due to turbulence model effects. The pressure change, of course, is also smeared over a finite distance. There is also some disagreement between analysis and experiment along the top wall near the inlet. This may be due to rapid changes in the wall contour in this region without sufficient mesh resolution.

The three runs for this case required 709.2, 679.3, and 694.4 seconds of CPU time, respectively, for execution on a Cray X-MP computer.

8.5 Example 2

In this example, computed results are presented for unsteady flow through the same diffuser used in Example 1. Extensive experimental measurements have been made by Sajben, Bogar, and Kroutil (1984) for a variety of unsteady flows through this diffuser. The results presented here are for an oscillating normal shock driven by an oscillating back pressure. The computations were again made using the Proteus Navier-Stokes code.

For this case, flow enters a converging-diverging duct at a Mach number of 0.47. It accelerates to supersonic conditions, then shocks down to subsonic conditions in the diverging part of the duct. The Mach number at the normal shock was about 1.25. The Reynolds number based on inlet height and velocity was 8.22×10^5. An 81 (streamwise) by 51 (cross-flow) mesh was used, packed in the streamwise direction near the expected location of the normal shock, and in the cross-flow direction near both walls. The inlet boundary conditions were specified total pressure p_T and total temperature T_T, zero cross-flow velocity v, and extrapolation of u. At the exit, the static pressure p_e was specified, and u, v, and the static temperature T were extrapolated. At the walls, no-slip adiabatic conditions were used, and the normal derivative of p was set equal to zero.

In the calculation, the exit pressure was first set at a low value to establish supersonic flow throughout the duct. Starting with zero velocity everywhere in the duct, steady conditions were obtained after 3000 time steps at a CFL number of 5.0. The exit pressure was then raised to $p_e/p_T = 0.82$, where p_T is the inlet total pressure. This was done gradually, taking 2000 time steps at a CFL number of 0.5. The CFL number was then raised to 5.0, and the calculation was continued until steady conditions were obtained after 16,000 additional time steps.

An oscillating exit pressure was then specified, using

$$\frac{p_e}{p_T} = \frac{(p_e)_0}{p_T} + a \sin(2\pi\omega t)$$

where $(p_e)_0/p_T = 0.82$ is the exit pressure at the start of the oscillation, $a = 0.01$ and $\omega = 100$ Hz are the amplitude and frequency of the oscillation, and t is the time from the start of the oscillation. The exit pressure p_e/p_T thus varied from 0.81 to 0.83. The calculation was continued for nine cycles, with 4000 time steps per cycle. The results for the last five cycles were examined closely and found to be essentially identical, indicating that periodic conditions have been achieved. The unsteady flow field will be presented in movie form. This calculation was run on a Cray X-MP computer, and used 6.7×10^{-5} seconds of CPU time per grid point per time step. The entire calculation thus required about 4.4 hours.

8.6 Example 3

In this example, computed results using Proteus are presented for viscous laminar flow past a circular cylinder. Although this is not an internal flow, it dramatically illustrates the complexity of flows that may be computed using a full time-averaged Navier-Stokes analysis.

In potential flow, the streamlines for flow past a circular cylinder are perfectly symmetric. The flow over the back half of the cylinder is a mirror image of the flow over the front half, with stagnation points at 0° and 180°. In real life, however, at Reynolds numbers Re_D larger than around 5, the flow separates from the surface, forming a wake. For Re_D between about 5 and 50, the flow is steady, with a pair of counter-rotating vortices in the wake near the cylinder. At Reynolds numbers larger than about 5000, the wake becomes fully turbulent. For Reynolds numbers between about 50 and 5000, however, the flow is laminar but unsteady. Vortices are alternately shed from the upper and lower surface, forming a Karman vortex street. This asymmetric flow is triggered by asymmetric perturbations inherent in any physical experiment.

The flow was run at $\mathrm{Re}_D = 100$. Incompressible conditions were approximated by using a free stream Mach number of 0.2. A polar grid was used, centered on the cylinder and extending to 30 cylinder radii. A 50 (radial) by 99 (circumferential) mesh was used, packed near the cylinder surface and the wake centerline.

The exact potential flow solution for flow over a cylinder was used for the initial flow field. At the cylinder surface, no-slip boundary conditions were used for the velocities u and v, and the derivative $\partial p/\partial r$ was set equal to

zero. At the outer boundary u, v, and p were set to vary smoothly from the fixed initial conditions to zero radial derivative conditions in the wake. Because the flow was expected to be asymmetric, implicit spatially periodic boundary conditions were used along the cut at the wake centerline.

As noted earlier, the asymmetric flow at this Reynolds number occurs in nature because of the asymmetries inherent in any physical experiment. However, in the computations the geometry, initial conditions, and boundary conditions are all symmetric. The Navier-Stokes equations should therefore lead to a symmetric flow at any Reynolds number. Round-off and truncation errors are, of course, asymmetric perturbations in a computation which could eventually lead to an asymmetric flow. Previous work has shown, however, that steady symmetric flow may be computed at Reynolds numbers as high as 1000. In the current calculation, therefore, an asymmetric perturbation was introduced using the following procedure.

From the initial flow field, 1000 time steps were taken at a CFL number, based on the minimum allowable time step, of 10. Second-order time differencing was used. The computed flow field at this point is symmetric. Asymmetry was introduced into the flow field at this time by temporarily rotating the cylinder first one direction, then the other. The solution was then continued at a CFL number of 5. The unsteady flow field will be presented in movie form.

9. REFERENCES

Abbott, J. M. (1977) ‘‘Aerodynamic Performance of a Scoop Inlet,’’ NASA TM 73725.

Anderson, B. H., and Benson, T. J. (1983) ‘‘Numerical Solution to the Glancing Sidewall Oblique Shock Wave/Turbulent Boundary Layer Interaction in Three Dimension,’’ AIAA Paper 83-0136 (also NASA TM 83056).

Anderson, D. A., Tannehill, J. C., and Pletcher, R. H. (1984) *Computational Fluid Mechanics and Heat Transfer*, Hemisphere Publishing Corporation, McGraw-Hill Book Company.

Baker, A. J. (1983) *Finite Element Computational Fluid Mechanics*, Hemisphere Publishing Corporation, McGraw-Hill Book Company.

Baldwin, B. S., and Lomax, H. (1978) ‘‘Thin Layer Approximation and Algebraic Model for Separated Turbulent Flows,’’ AIAA Paper 78-257.

Briley, W. R., and McDonald, H. (1979) ‘‘Analysis and Computation of Viscous Subsonic Primary and Secondary Flows,’’ AIAA Paper 79-1453.

Buggeln, R. C., McDonald, H., Kreskovsky, J. P., and Levy, R. (1979) ‘‘Development of a Three-Dimensional Supersonic Inlet Flow Analysis,’’ NASA CR 3218.

Buggeln, R. C., McDonald, H., and Kim, Y.-N. (1983) ‘‘Computation of Multi-Dimensional Viscous Supersonic Flow by Spatial Forward Marching,’’ AIAA Paper 83-0177.

Cebeci, T., Kaups, K., Mosinskis, G. J., and Rehn, J. A. (1973) ‘‘Some Problems of the Calculation of Three-Dimensional Boundary Layer Flows on General Configurations,’’ NASA CR-2285.

Denton, J. D. (1982) ‘‘An Improved Time Marching Method for Turbomachinery Calculation,’’ ASME Paper 82-GT-239.

Denton, J. D. (1983) Lecture Notes, ASME Turbomachinery Institute Course on Fluid Dynamics of Turbomachinery, July 18–27.

Fletcher, C. A. J. (1988) *Computational Techniques for Fluid Dynamics, Volumes 1 and 2*, Springer-Verlag.

Hess, J. L., Mack, D.-P., and Stockman, N. O. (1979) ‘‘An Efficient User-Oriented Method for Calculating Compressible Flow In and About Three-Dimensional Inlets,’’ NASA CR 159578.

Hoffmann, K. A. (1989) *Computational Fluid Dynamics for Engineers*, Engineering Education System.

Hsieh, T., Wardlaw, A. B., Jr., Collins, P., and Coakley, T. J. (1987) ‘‘Numerical Investigation of Unsteady Inlet Flow Fields,’’ AIAA Journal, Vol. 25, No. 1, pp. 75–81.

Kao, H. C. (1981) ‘‘Some Aspects of Calculating Flows About Three-Dimensional Subsonic Inlets,’’ NASA TM 82678.

Koncsek, J. L. (1975) ‘‘Machine Plot Supplement to D6-42494,’’ Rept. D6-42595, The Boeing Company, Seattle, Wash.

Levy, R., Briley, W. R., and McDonald, H. (1983) ‘‘Viscous Primary/Secondary Flow Analysis for Use with Nonorthogonal Coordinate Systems,’’ AIAA Paper 83-0556.

Levy, R., McDonald, H., Briley, W. R., and Kreskovsky, J. P. (1980) ‘‘A Three-Dimensional Turbulent Compressible Subsonic Duct Flow Analysis for Use with Constructed Coordinate Systems,’’ AIAA Paper 80-1398.

Lieblein, S., and Stockman, N. O. (1972) ‘‘Compressibility Correction for Internal Flow Solutions,’’ Journal of Aircraft, Vol. 9, No. 4, pp. 312–313.

McDonald, H., and Camarata, F. J. (1969) ‘‘An Extended Mixing Length Approach for Computing the Turbulent Boundary Layer Development,’’ *Computation of Turbulent Boundary Layers — 1968 AFOSR-IFP-Stanford Conference*, S. J. Kline, et. al., eds., Stanford University, pp. 83–98.

Oskam, B., Vas, I. E., and Bogdonoff, S. M. (1976) ‘‘Mach 3.0 Oblique Shock Wave/Turbulent Boundary Layer

Interactions in Three Dimensions,'' AIAA Paper 76-336.

Pierzga, M. J., and Wood, J. R. (1985) ''Investigation of the Three-Dimensional Flow Field Within a Transonic Fan Rotor: Experiment and Analysis,'' Journal of Engineering for Gas Turbines and Power, Vol. 107, pp. 436–449.

Reyhner, T. A. (1982) ''Computation of Transonic Potential Flow About Three-Dimensional Inlets, Ducts, and Bodies,'' NASA CR 3514.

Reyhner, T. A., and Flugge-Lotz, I. (1968) ''The Interaction of a Shock Wave with a Laminar Boundary Layer,'' International Journal of Non-Linear Mechanics, Vol. 3, pp. 173–199.

Sajben, M., Bogar, T. J., and Kroutil, J. C. (1984) ''Forced Oscillation Experiments in Supercritical Diffuser Flows,'' AIAA Journal, Vol. 22, No. 4.

Syberg, J., and Koncsek, J. L. (1975) ''Experimental Evaluation of a Mach 3.5 Axisymmetric Inlet,'' NASA CR 2563.

Towne, C. E., and Flitcroft, J. E. (1986) ''Analysis of Intake Ducts Using a Three-Dimensional Viscous Marching Procedure,'' Presented at the First World Congress on Computational Mechanics, The University of Texas at Austin, Sept. 22–26.

Towne, C. E., Schwab, J. R., and Bui, T. T. (1993a) ''Proteus Two-Dimensional Navier-Stokes Computer Code — Version 2.0, Volumes 1–3,'' NASA TM's 106336, 106338, 106339.

Towne, C. E., Schwab, J. R., and Bui, T. T. (1993b) ''Proteus Three-Dimensional Navier-Stokes Computer Code — Version 1.0, Volumes 1–3,'' NASA TM's 106337, 106340, 106341.

Vadyak, J., Hoffman, J. D., and Bishop, A. R. (1984) ''Three-Dimensional Flow Simulations for Supersonic Mixed-Compression Inlets at Incidence,'' AIAA Journal, Vol. 22, No. 7, pp. 873–881.

Willmer, A. C., Brown, T. W., and Goldsmith, E. L. (1981) ''Effects of Intake Geometry on Circular Pitot Intake Performance at Zero and Low Forward Speeds,'' *Aerodynamics of Power Plant Installation,* AGARD CP 301, Paper No. 5.

10. BIBLIOGRAPHY

Anderson, D. A., Tannehill, J. C., and Pletcher, R. H. (1984) *Computational Fluid Mechanics and Heat Transfer*, Hemisphere Publishing Corporation, McGraw-Hill Book Company.

Baker, A. J. (1983) *Finite Element Computational Fluid Mechanics*, Hemisphere Publishing Corporation, McGraw-Hill Book Company.

Ballhaus, W. F. (1982) ''Computational Aerodynamics and Design,'' *Lecture Notes in Physics, Eighth International Conference on Numerical Methods in Fluid Dynamics*, Springer-Verlag.

Cebeci, T., and Smith, A. M. O. (1974) *Analysis of Turbulent Boundary Layers*, Academic Press.

Chapra, S. C., and Canale, R. P. (1988) *Numerical Methods for Engineers*, McGraw-Hill.

Fletcher, C. A. J. (1988) *Computational Techniques for Fluid Dynamics, Volumes 1 and 2*, Springer-Verlag.

Hirsch, C. (1988) *Numerical Computation of Internal and External Flows, Volume 1: Fundamentals of Numerical Discretization*, John Wiley & Sons, Inc.

Hirsch, C. (1990) *Numerical Computation of Internal and External Flows, Volume 2: Computational Methods for Inviscid and Viscous Flows*, John Wiley & Sons, Inc.

Hoffmann, K. A. (1989) *Computational Fluid Dynamics for Engineers*, Engineering Education System.

Krause, E. (1985) ''Computational Fluid Dynamics: Its Present Status and Future Direction,'' Computers and Fluids, Vol. 13, No. 3, pp. 239–269.

Kutler, P. (1983) ''A Perspective of Theoretical and Applied Computational Fluid Dynamics,'' AIAA Paper 83-0037.

Murthy, S. N. B., and Paynter, G. C., eds. (1986) *Numerical Methods for Engine-Airframe Integration*, Progress in Astronautics and Aeronautics, Vol. 102, AIAA.

Povinelli, L. A. (1984) ''Assessment of Three-Dimensional Inviscid Codes and Loss Calculations for Turbine Aerodynamic Computations,'' NASA TM 83571.

Povinelli, L. A. (1986) ''Validation of Viscous and Inviscid Computational Methods for Turbomachinery Components,'' ASME Paper 86-GT-42.

Povinelli, L. A., and Towne, C. E. (1986) ''Viscous Analyses for Flow Through Subsonic and Supersonic Intakes,'' NASA TM 88831.

Shang, J. S. (1985) ''An Assessment of Numerical Solutions of the Compressible Navier-Stokes Equations,'' Journal of Aircraft, Vol. 22, No. 5, pp. 353–370.

Zucrow, M. J., and Hoffman, J. D. (1976) *Gas Dynamics, Volumes 1 and 2*, John Wiley & Sons, Inc.

CONTENTS